Chapter 8

Central Calorimeter

8.1 Introduction

The CDF central calorimeter is retained largely unchanged other than electronics for Run II. It is a scintillator sampling system with tower segmentation; each tower is 15 degrees in azimuth by about 0.11 in pseudorapidity. Each wedge consists of a lead-scintillator E–M section backed by a steel-scintillator central hadron calorimeter. The wedges are assembled into central arches. The endwall hadron calorimeter consists of modules mounted to the solenoid flux return to provide hadronic coverage from 30° to 45° on both sides.

The PMT energy measurements are fast enough to take full advantage of the Run II 132 ns bunch structure. The wire chambers associated with the E–M calorimeter may need to be integrated over several crossings but their fine granularity implies a low enough occupancy that this should not be a significant problem.

In Run Ib we have a sample of data of average instantaneous luminosity about $10^{31} cm^{-2} sec^{-1}$, which for PMTs corresponds to 6×10^{31} and 1.8×10^{32} for 36 and 108 bunches respectively. These correspond to an average of about 0.9 extra overlying minimum bias events. A minimum bias event on average contributes roughly 15 MeV to a $15° \delta\phi \times 0.11 \delta\eta$ calorimeter tower. For jets, by making the underlying cone correction appropriately luminosity dependent we largely retain the quality of the jet measurements. Inclusive electrons at about 10 GeV E_T see an effective luminosity dependent pedestal shift of up to a few tenths of a per cent for the usual three tower electron energy definition; there should be no significant impact on physics measurements.

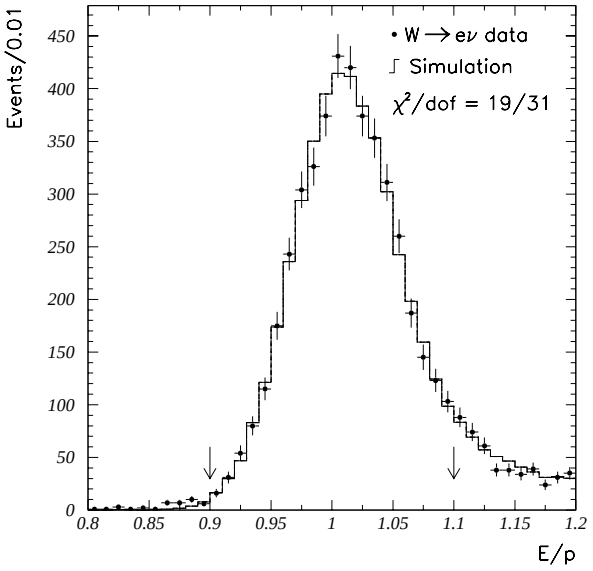

Figure 8.1: Energy over momentum for electrons in the Ia W mass sample. The peak fit region is marked.

8.2 Central E–M Calorimeter

Each 15° wedge has alternating lead and scintillator with an imbedded two dimensional readout strip chamber at shower maximum.[1] Wavelength shifters at the ϕ surfaces direct the light to (Hamamatsu R580) PMTs.[2] Energy resolution in the central electromagnetic calorimeter should be dominated by sampling. The thickness of the lead used in its construction corresponds to $11.6\%/\sqrt{E_T}$. The design specification of more than 100 pe/GeV/tube resulted in a test beam resolution of $13.5\%/\sqrt{E_T}$ which we use as the nominal stochastic resolution. Source calibrations are used to retain testbeam calibration from initial settings[3]; these continue to allow startup with individual tower gains accurate to $\sim \pm 3\%$ and within 2% for overall absolute scale. The source system

is complemented by xenon and LED light flashers, which are useful in diagnosis of problems.

The EM calorimeter, along with tracking and hadron calorimeter, has provided effective identification of electrons[4] and photons[5]. Imperfect corrections for the small variations across the face of a calorimeter cell[6] as well as the statistical error and time drifts in setting individual tower gain calibration result in a constant term in the energy resolution. Calibration of the calorimeter *in situ* has used tracking information in inclusive electrons to determine relative gains and tracking for W electrons to set the absolute energy scale. We measure the tracking material using the E/p tail or conversions and use a radiative Monte Carlo to match the E/p peak as shown in Fig. 8.1. The effective constant term in resolution has been $\pm 2\%$ or less and the absolute energy scale for the W mass measurement is known to $\pm 0.15\%$ for Ia.[7]

The scintillator used is SCSN-38 and the wavelength shifter used is Y7 PMMA; neither should be a radiation damage problem for any luminosity scenario. We have tracked the response since the modules have been assembled, and whether there is beam or not, there is a light yield loss of about 1% per year. About 60% of the loss is directly explained by the gradual shortening of the effective attenuation length of the scintillator as seen in Fig. 8.2. This trend has continued through Ia and Ib.

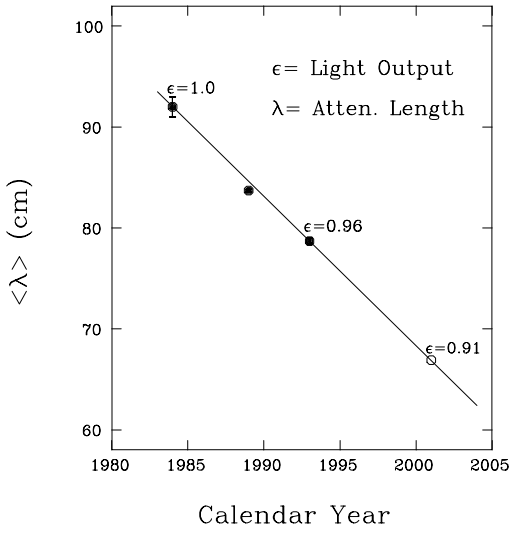

Figure 8.2: Scintillator attenuation length versus year. The observed trend corresponds to 0.6% light loss per year due to transmission loss in the scintillator.

There is a tendency during data taking for gain to fall more rapidly than the nominal during running with some recovery at shutdowns. This is illustrated for Run Ib in Fig. 8.3. These trends are correlated to calorimeter arches which are thermal masses and share common high voltage supply. The gains are monitored using E/p for inclusive electrons. Run number is a reasonably constant clock and the span is 18 months. The dip in the SE arch was an excursion in high voltage. If there is 20% less light yield than design in 2005, the stochastic resolution would only degrade from 13.5 to $14\%/\sqrt{E_T}$. The effect on the response map is readily monitored and accounted.

The shower maximum chambers have contributed quite effectively to identification of electrons and photons, using the position measurement to match with tracks, the transverse shower profile to separate photons from π^0s, and pulse height to help identify electromagnetic showers. Similar functionality has been proposed for most calorimeters considered since CDF demonstrated the efficacy of a 2 dimensional fine shower maximum detector.

In order to increase available trigger bandwidth some of the shower maximum functionality has recently been implemented into the level 2 trigger.[8] This gave a factor of 2 reduction in electron candidate bandwidth with little loss of signal. This functionality will be expanded in the Run II trigger.

Each gap between adjacent wedge modules is covered by a 12 X_0 tungsten bar backed by a wire chamber. The tungsten serves to recover some of the response for particles, particularly photons, which might otherwise escape completely. The chamber resolution and noise has been too poor to include in energy measurements but the information has been valuable in studying the occasional odd event.

Since the beginning of Run Ia the photon and soft electron identification has been greatly enhanced by preshower wire chambers mounted on the front of the wedges, using the coil and tracking material as a radiator. For example, in the top quark analysis,[9] the soft electron b tagging algorithm uses the CPR to gain a factor of 2 rejection of electron backgrounds after all other identification cuts are applied, while maintaining high efficiency for true electrons. This is illustrated in Fig. 8.4, where the CPR response for a) random tracks that are predominantly pions,

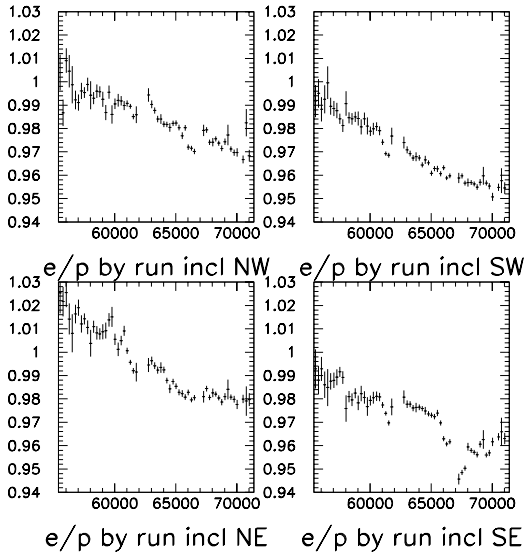

Figure 8.3: Central electromagnetic calorimeter gains by arch (quadrant in the horizontal plane) versus run for Ib (18 months) for inclusive electrons.

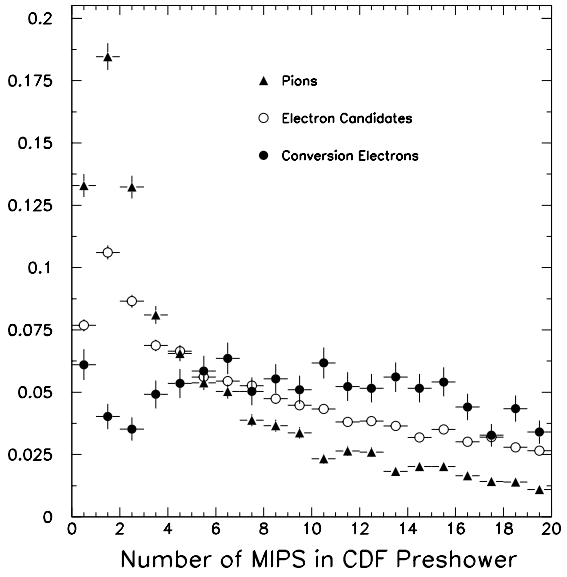

Figure 8.4: The response of the preshower detector to pions, electrons, and electron candidates.

b) pure electrons from conversions, and c) electron candidates that pass all other identification cuts is shown.

In addition, the CPR has been responsible for reducing the systematic uncertainties for direct photon measurements by a factor of 3, giving CDF the most precise measurement of direct photons, as well as extending the measurement in E_T beyond the capability of shower profile measurements.[10] The crucial 1% calibration of the material in front of CPR was performed with reconstructed π^0, η, ρ mesons shown in Fig. 8.5.

The wire chamber readout will be concurrent with digital traffic in the Run II DAQ system so steps are being taken to minimize noise sensitivity. One hopes that the Run II noise levels will not be significantly worse and tests using noise sources have been encouraging.

There is no sign of aging in either shower max or preshower wire chambers. Extrapolation can be made from the current which is drawn during running; one expects about 0.1 mC/cm/fb^{-1} for shower max and 9 mC/cm/fb^{-1} for preshower chambers. Bench tests show little gain loss to 0.4 C/cm.

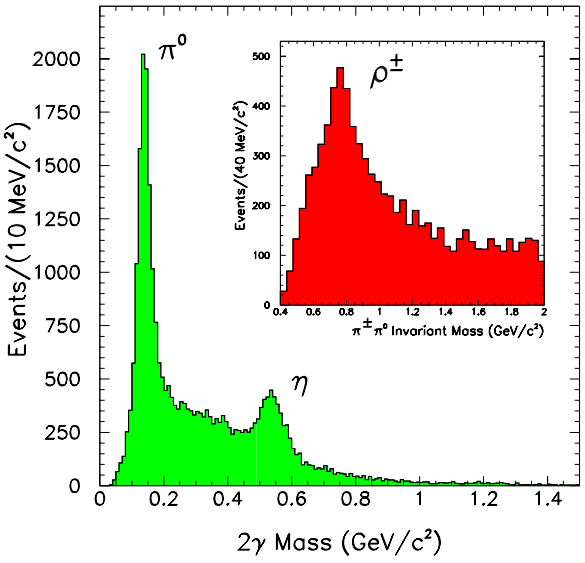

Figure 8.5: The calibration of preshower material was performed with the reconstructed meson peaks as shown.

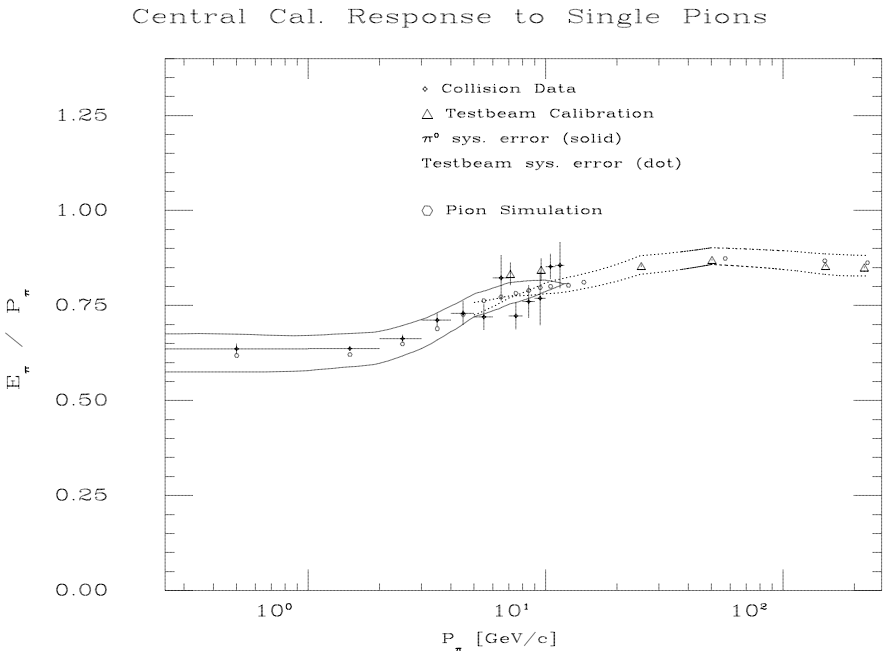

Figure 8.6: Central calorimeter response to pions from test beam measurements and *in situ* isolated particle measurements. The overall level is an artifact of the convention of calibrating the hadron towers in the testbeam using 50 GeV/c pions which were minimum ionizing in the E–M section. The nonlinearity is a characteristic of the lack of compensation in the combined lead and iron calorimeters.

8.3 Central and Endwall Hadron Calorimeters

The central and endwall hadron calorimeters are composed of alternating layers of iron and scintillator. Fingers of wavelength shifter are configured much as fibers are in more recent scintillator calorimeters.[11] Similar to the E–M, the basic calibration is extrapolated from the testbeam using source response. The central hadron calorimeter shares the source drive systems with the E–M. The endwall hadron calorimeter uses a seperate set of sources drives, one per endwall. Operational monitoring is done using a laser flasher system. The test beam calibration is complemented by *in situ* studies using isolated tracks, as shown in Fig. 8.6. Detector systematics are folded in with other systematics in measuring jet energies.[12] These systematics are important for measuring the central jet E_T spectrum[13]. Dijet balance is used to transfer the central calibration to the overall calorimeter. The tracking and EM scales are compared to the jet measurement using photon jet as Z^0 jet balance, shown in Fig 8.7. This confirms the jet energy scale overall

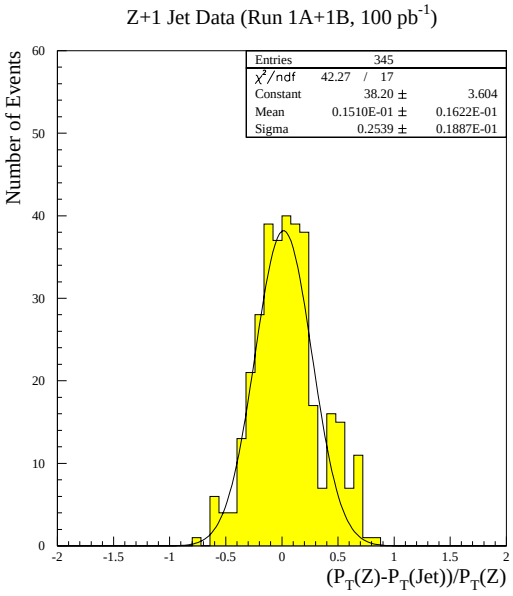

Figure 8.7: Discrepancy between the lepton measurement and the CDF calorimeter in Z plus two jet events.

which is important for measuring the top mass.[9]

The hadron calorimeters use PMMA naphthalene scintillator which should not be sensitive to radiation damage directly from luminosity. Removal of the main ring and attention to shielding from beam halo and other external sources of radiation will be necessary for the survival of this scintillator through Run II. The PMTs, Thorn-EMI 9954 central and Thorn-EMI 9902 endwall, are currently stabilized by running LEDs between bunches; perhaps some scheme for running the LEDs during the abort gaps may be effective or perhaps the PMTs need to be replaced.

Bibliography

[1] L. Balka *et al.*, NIMPR **A267** (1988) 272, L. Nodulman *et al.*, NIM **204** (1983) 351, T. Kamon *et al.*, NIM **213** (1983) 61.

[2] T. Devlin *et al.*, NIMPR **A268** (1988) 209.

[3] S. Hahn *et al.*, NIMPR **A267** (1988) 351.

[4] F. Abe *et al.*, Phys. Rev. **D44** (1991) 91.

[5] F. Abe *et al.*, Phys. Rev. **D48** (1993) 2998.

[6] K. Yasuoka *et al.*, NIMPR **A267** (1988) 315.

[7] F. Abe *et al.*, Phys. Rev. **D43** (1991) 2070, F. Abe *et al.*, Phys. Rev. **D52** (1995) 4784.

[8] K. Byrum *et al.*, NIMPR **A364** (1995) 144.

[9] F. Abe *et al.*, Phys. Rev. **D50** (1994) 2296.

[10] F. Abe *et al.*, Phys. Rev. Lett. **73** (1994) 2662.

[11] S. Bertolucci *et al.*, NIMPR **A267** (1988) 301.

[12] F. Abe *et al.*, Phys. Rev. **D45** (1992) 1448, F. Abe *et al.*, Phys. Rev. Lett. **65** (1990) 968.

[13] F. Abe *et al.*, Phys. Rev. Lett. **62** (1989) 613, F. Abe *et al.*, Phys. Rev. Lett. **68** (1992) 1104, F. Abe *et al.*, Phys. Rev. Lett. **77** (1996) 438.